Sustained Connexin43 Mimetic Peptide Release From Loaded Nanoparticles Reduces Retinal and Choroidal Photodamage

Nasir Mat Nor,[1–3] Cindy X. Guo,[1,3] Ilva D. Rupenthal,[3–5] Ying-Shan Chen,[3–5] Colin R. Green,[3,4] and Monica L. Acosta[1,3]

[1]School of Optometry and Vision Science, University of Auckland, Auckland, New Zealand
[2]Faculty of Medicine, University of Sultan Zainal Abidin, Kuala Terengganu, Malaysia
[3]New Zealand National Eye Centre, University of Auckland, Auckland, New Zealand
[4]Department of Ophthalmology, University of Auckland, Auckland, New Zealand
[5]Buchanan Ocular Therapeutics Unit, University of Auckland, Auckland, New Zealand

Correspondence: Monica L. Acosta, School of Optometry and Vision Science, University of Auckland, Private Bag 92019, Auckland 1142, New Zealand; m.acosta@auckland.ac.nz.

Submitted: August 21, 2017
Accepted: May 31, 2018

Citation: Mat Nor N, Guo CX, Rupenthal ID, Chen Y-S, Green CR, Acosta ML. Sustained connexin43 mimetic peptide release from loaded nanoparticles reduces retinal and choroidal photodamage. *Invest Ophthalmol Vis Sci*. 2018;59:3682–3693. https://doi.org/10.1167/iovs.17-22829

Purpose. To evaluate the long-term effect on inflammation and inflammasome activation of intravitreally delivered connexin43 mimetic peptide (Cx43MP) in saline or incorporated within nanoparticles (NPs) for the treatment of the light-damaged rat eye.

Methods. Light-induced damage to the retina was created by exposure of adult albino Sprague-Dawley rats to intense light for 24 hours. A single dose of Cx43MP, Cx43MP-NPs, or saline was injected intravitreally at 2 hours after onset of light damage. Fluorescein isothiocyanate (FITC)-labelled Cx43MP-NPs were intravitreally injected to confirm delivery into the retina. Electroretinogram (ERG) recordings were performed at 24 hours, 1 week, and 2 weeks post cessation of light damage. The retinal and choroidal layers were analyzed in vivo using optical coherence tomography (OCT) and immunohistochemistry was performed on harvested tissues using glial fibrillary acidic protein (GFAP), leukocyte common antigen (CD45), and Cx43 antibodies.

Results. FITC was visualized 30 minutes after injection in the ganglion cell layer and in the choroid. Cx43MP and Cx43MP-NP treatments improved a-wave and b-wave function of the ERG compared with saline-injected eyes at 1 week and 2 weeks post treatment, and prevented photoreceptor loss by 2 weeks post treatment. Inflammation was also reduced and this was in parallel with downregulation of Cx43 expression.

Conclusions. The slow release of Cx43MP incorporated into NPs is more effective at treating retinal injury than a single dose of native Cx43MP in solution by reducing inflammation and maintaining both retinal structure and function. This NP preparation has clinical relevance as it reduces possible ocular complications associated with repeated intravitreal injections.

Keywords: choroid, retina, light damage, connexins, retinal degeneration

Inflammation plays a significant role in the development of the pathogenesis of age-related macular degeneration (AMD).[1–3] In AMD, local inflammation is associated with an immune cell–mediated process that leads to a chronic inflammatory environment.[4] According to recent reports, the inflammatory reaction is associated with an increase in connexin43 (Cx43) expression, primarily in the choroid, RPE, and retina.[5] Cx43 forms gap junctions that play a major role in the bidirectional movement of ions and metabolites between cells, contributing to the blood-retinal barrier in endothelial cells.[6–10] However, Cx43 also forms hemichannels in the plasma membrane, including that of endothelial cells and astrocytes in response to injury, and these "pathological pores" play a major role in the inflammatory reaction and its perpetuation.[11–17] This has been demonstrated in experiments in which connexin channel-blocking mimetic peptides have been used to prevent connexin hemichannel opening and reduce the inflammatory response.[5,18–25] However, the short half-life of native Cx43 mimetic peptides[26] in solution is potentially an obstacle for long-term therapeutic effects.

One Cx43 mimetic peptide (Cx43MP), also known as peptide5, is a short amino acid sequence of the extracellular loop of rat Cx43.[27] This peptide can be delivered directly into the eye via intravitreal (IVT), subtenon or intravenous injections.[28–30] The main advantage of IVT injection is that it provides a localized concentration of drug that diffuses directly to posterior segment tissues with minimal systemic side effects.[30–32] IVT injection is the preferred and standard drug delivery method to treat posterior eye segment diseases, enabling the direct delivery of molecules with high molecular mass.[33] However, in the treatment of certain conditions, repeated IVT injections are required to maintain drug availability and thus treatment efficacy, which may lead to a number of ocular complications such as subconjunctival hemorrhages, vitreous hemorrhage, endophthalmitis, retinal detachment, or cataract formation.[28,29]

Copyright 2018 The Authors

This work is licensed under a Creative Commons Attribution-NonCommercial-NoDerivatives 4.0 International License.

Downloaded From: https://iovs.arvojournals.org/pdfaccess.ashx?url=/data/journals/iovs/937362/ on 07/20/2018

Advances have been made in formulations that protect the active ingredient from enzymatic degradation and allow slow drug release over time.[21,34] Nanoparticles (NPs) are one of the most widely used groups of drug delivery systems. A large number of studies have described the potential for polymeric NPs to be used in the treatment of retinal diseases because of their high tolerance, biocompatibility, biodegradability, and lack of intrinsic immunogenicity.[21,35,36] We have previously shown that a double injection of unmodified Cx43MP is protective against damage in the intense light–exposed rat retina.[5] In this study we investigated the effect of sustained Cx43MP delivery from NPs and monitored the effect on inflammation, as well as connexin expression that occurs in the light-damaged rat retina.

Materials and Methods

Light Damage Procedure

Six- to eight-week-old Sprague-Dawley (SD) rats (200–250 g; male or female) were used in this experiment. All experimental procedures were approved by the University of Auckland Animal Ethics Committee (approval No. 001462) and complied with the ARVO Statement for the Use of Animals in Ophthalmic and Vision Research. SD rats were obtained from the Vernon Jansen Unit, the University of Auckland. Light damage was induced using a light source with a luminance of 2700 lux from fluorescent light lamps with no heat emission (Philips Master TLD 18W/965, 380–760 nm; Koninklijke Philips Electronics N.V., Shanghai, China) when placed directly above the rat cage. Animals were allowed to roam free in the cages during light exposure and had ad libitum access to food and water. Light damage experiments were performed consistently starting at 9:00 AM. After the 24 hours of intense light exposure, animals were returned to normal light/dark cycle conditions of 12 hours of light (174 lux) and 12 hours of darkness (<62 lux). Figure 1 shows the experimental setup and the outline of the intervention protocols.

Animal Anesthesia

For IVT injections and ERG recordings animals were anesthetized by intraperitoneal (i.p.) injection using a combination of ketamine (75 mg/kg; Parnell Technologies, Auckland, New Zealand) and Domitor (0.5 mg/kg; Pfizer, Auckland, New Zealand). Following manipulations, anesthesia was reversed by intraperitoneally injecting atipamezole (1 mg/kg Antisedan, Pfizer) and animals were returned back to their cages. Warm water bottles were used to maintain the animals' body temperature during recovery.

Mimetic Peptide Preparation and Intravitreal Injections

Poly-(d, l-lactic-co-glycolic acid) (PLGA, 50 lactic:50 glycolic acid; Sigma-Aldrich, Auckland, New Zealand) NPs were prepared according to the procedure described by Chen et al.[21,37] using the double emulsion solvent evaporation method.[26,37] Briefly, the 5 mM Cx43MP (MWt 1396 g/mol; Auspep, VIC, Australia) aqueous solution was emulsified in dichloromethane containing 30 mg/mL PLGA using a probe sonicator (amplitude 50 W; duty cycle 0.6 s/min; Hielscher, Teltow, Germany) to agitate particles and form the primary water-in-oil (w/o) emulsion. The primary w/o emulsion then underwent a second emulsification in 3% wt/vol polyvinyl alcohol (PVA) (Sigma-Aldrich, New Zealand) aqueous solution to form a water-in-oil-in-water (w/o/w) emulsion, which was then poured into a 0.1% wt/vol aqueous PVA solution. This procedure was performed to stabilize the double emulsion during the evaporation process and was followed by ultracentrifugation using a ProteomeLab XL-A/XL-I, Type 70 Ti rotor (Beckman Coulter, Auckland, New Zealand) at 11,000*g* and 4°C. Formed Cx43MP-NPs were then lyophilized (VirTis) (SP Scientific, Gardiner, USA) for 24 hours.

Both the Cx43MP-NPs and the Cx43MP formulations were diluted in saline to a final peptide concentration of 280 μM. This peptide concentration was chosen based on previous intervention studies using the light-damaged rat model.[11] Previous studies have shown that PLGA injected intravitreally does not result in any electrophysiological or histologic toxicity in the retina.[38,39] Thus, saline was used as injection control, given the extensive previous evaluation and feasibility regarding PLGA NPs as suitable vehicles for ophthalmic administration.[40–44] Treatment consisted of 4 μL Cx43MP, Cx43MP-NPs, or saline injected into the vitreous 2 hours after the onset of intense light exposure. A Hamilton syringe attached to a 30-gauge × 0.5-inch needle (BD PrecisionGlide; Becton, Dickinson and Company, Franklin Lakes, NJ, USA) was used for the injection. In order to avoid damage to the lens, the injections were made into the temporal side of the eye after rotating the eyeball to the nasal side by holding the bulbar conjunctiva. Maxitrol (Alcon, Fort Worth, TX, USA) was also applied to the cornea after the IVT injection to avoid any ocular infection at the site of injection.

Electroretinogram

The procedure was performed as described previously.[11,45] SD rats were dark-adapted overnight for 12 to 14 hours before the ERG recording. The ERG baseline was recorded before light damage and again at 24 hours, 1 week, and 2 weeks after the cessation of the light damage procedure. A dim red light generated by a light-emitting diode ($\lambda max = 650$ nm) was used during manipulations of dark-adapted animals. The corneas were maintained hydrated with 1% carboxymethylcellulose sodium (Celluvisc; Allergan, Irvine, CA, USA) throughout the whole ERG recording. Right- and left-eye ERGs were recorded at the same time. The active electrodes were gold ring electrodes (Roland Consult Stasche & Finger GmbH, Brandenburg, Germany) and were placed in contact with the center of the cornea. The inactive electrode was hooked around the front teeth and in contact with the wet tongue. Body temperature was kept approximately at 37°C to avoid temperature-driven ERG amplitude fluctuations.

Full-field ERG responses were elicited by a twin-flash (0.8-ms stimulus interval) generated from a photographic flash unit (Nikon SB900 Flash, Tokyo, Japan), via a Ganzfeld sphere. In the Ganzfeld method, an integrating sphere approximately 650 cm in diameter, painted white internally, was used to reflect the light onto the dilated pupil. The flash intensity range was from −2.9 to 2.1 log candela-seconds per meter squared (cd.s/m^2) and was attenuated using neutral density filters (Kodak Wratten; Eastman Kodak, Rochester, NY, USA) in order to obtain light intensities of −3.9, −2.9, −1.9, 0.1, 1.1, 1.6, 1.8, and 2.1 log cd.s/m^2. The flash intensity was calibrated using an IL1700 research radiometer (UV Process Supply, Inc., Chicago, IL, USA). This study utilized a twin-flash paradigm for the isolation of rod and cone pathways. Paired flashes of identical luminous energy were triggered from the flash unit. The rod and cone mixed responses were recorded after the initial flash, and the response from the second flash was recorded representing the function from cones only. The rod PIII response was derived through digital subtraction of the cone response

Investigative Ophthalmology & Visual Science

Downloaded From: https://iovs.arvojournals.org/pdfaccess.ashx?url=/data/journals/iovs/937362/ on 07/20/2018

Table 1. List of Primary Antibodies Used in Immunohistochemistry

Antibody	Production	Host	Working Dilution	Supplier	Cat. No.	Immunogen	Reference
Anti-Cx43	Polyclonal	Rb	1:1000	Sigma-Aldrich, USA	C6219	Synthetic peptide corresponding to amino acids 363–382 of human and rat Cx	11, 73
Anti-GFAP	Monoclonal, clone G-A-5 Cy3-conjugated	Ms	1:1000	Sigma-Aldrich, USA	C9205	The carboxy terminal Cys II fragment and the N-terminal part of GFAP	5, 70
Anti-CD45	Monoclonal, clone OX-1	Ms	1:20	BD Pharmingen	550566	CD 45-enriched glycoprotein fraction from Wistar rat thymocytes	5

from the initial mixed response. Recordings were performed in a Faraday cage to reduce electrical noise. The results of ERG signals were amplified 1000 times by a Dual Bio Amp (AD Instruments, NSW, Australia), and waveforms were recorded by using the Scope software (AD Instruments, Dunedin, New Zealand) and analyzed using published algorithms of the amplitudes of a-wave and b-wave.[5,45]

Optical Coherence Tomography

The optical coherence tomography (OCT) imaging technique was used to obtain information on in vivo retinal layers and choroid structure. Spectral-domain optical coherence tomography (SD-OCT, Micron IV; Phoenix Research Laboratories, Pleasanton, CA, USA) was employed. This procedure was executed immediately after ERG recordings under anesthesia and pupil dilation.[5] Rats were placed on a 37°C heating pad to maintain their body temperature and to prevent the development of cold cataracts. Dilated eyes were covered with Poly Gel (3 mg/g Carbomer; Alcon, NSW, Australia) and the retina was visualized by contacting the OCT lens to the gel. StreamPix 6 software, version 7.2.4.2 (Phoenix Research Laboratories) was used in image acquisition. The SD-OCT ultra-broadband (160 nm) light source was used to obtain 1024 pixels per A-scan and 10 frames per horizontal B-scan with 2-μm axial resolution. Images were acquired 2 mm from the optic nerve in the dorsal retina. Images were analyzed using InSight software, version 1.1.5207 (Phoenix Research Laboratories) to calculate the thickness of retinal layers and choroid. The choroid was measured from the hyperreflective Bruch's membrane to the choroidal vessels and the sclera intersection. The outer nuclear layer was measured from the RPE hyperreflective line to the outer plexiform layer (OPL) interface.

Animal Tissue Collection and Processing

After the final ERG recording (2 weeks post light damage), deeply anesthetized rats were perfused transcardially with saline for 2 to 3 minutes followed by 30-minute perfusion with 4% paraformaldehyde (PFA) in 0.1 M phosphate buffer (PB). The eyes were dissected from the orbit; eyecups were further fixed in 4% PFA for 30 minutes and then washed in 0.1 M phosphate-buffered saline (PBS), pH 7.4. Tissues were either prepared for whole-mount immunohistochemistry or prepared for freezing and sectioning. For the latter, tissues were cryoprotected by passing them through increasing concentrations of sucrose solution up to 30% (wt/vol). They were then submerged in optimal cutting temperature medium (OCT; Sakura Finetek, Torrance, CA, USA) and frozen. Cryosections were 12 μm in thickness and were collected on Super-Frost Plus slides (Labserv, Auckland, New Zealand) for immunohistochemical labelling.

FITC-Cx43MP-NP Detection in Whole-Mount Tissues

The diffusion of fluorescein isothiocyanate (FITC)-conjugated Cx43MP loaded into PLGA NPs was assessed in whole-mount tissues and in sections following IVT injection. A volume of 4 μL FITC-conjugated Cx43MP-NPs (280 μM) was injected into the vitreous immediately after 24 hours of intense light exposure. Tissues were collected 30 minutes post injection, fixed in 4% PFA for 30 minutes, washed with PBS, and then stained for 2 minutes with 4′,6-diamidino-2-phenylindole dihydrochloride (DAPI; 1:1000; Sigma-Aldrich Corp., St. Louis, MO, USA). Whole-mount tissue and sections were mounted in antifading medium (CitiFluor Ltd., Leicester, UK) and were visualised using an Olympus FV1000 Confocal Microscope (Olympus, Tokyo, Japan).

Immunohistochemical Labelling of Tissue Sections

Immunohistochemical labelling was conducted using the indirect immunofluorescence technique. Briefly, frozen tissue sections were air-dried at room temperature for 10 to 15 minutes and washed with 0.1 M PBS. The tissue sections were blocked with a solution containing 6% normal goat serum or donkey serum (Invitrogen, Grand Island, NY, USA), 1% bovine serum albumin (BSA; Sigma-Aldrich, New Zealand) and 0.5 % Triton X-100 in 0.1 M PBS for 1 hour at room temperature. The tissues were immunolabelled with primary antibodies, including rabbit anti-Cx43 mouse anti-leukocyte common antigen (CD45) and mouse anti-glial fibrillary acidic protein (GFAP) antibodies (Table 1), and were incubated overnight at room temperature. After the incubation period, sections were washed four times for 15 minutes each in 0.1 M PBS in order to remove excess primary antibody. The secondary antibody, goat anti-rabbit or goat anti-mouse, conjugated with Alexa 488 or Alexa 594 (Molecular Probes, Thermo Fisher Scientific, Auckland, New Zealand) was diluted 1:500 and incubated for 2 to 3 hours in the dark at room temperature. The slides were washed thoroughly with 0.1 M PBS to remove excess secondary antibody. Slides were mounted in CitiFluor and sealed with nail polish.

Statistical Analysis

Graphing and statistical analyses were performed using GraphPad Prism 5 (GraphPad Software, La Jolla, CA, USA). All data are presented as mean ± the standard error of the mean (SEM). Functional and morphologic data ($n = 6$ per group) were compared using analysis of variance with an α value of 0.05. A 2-way ANOVA followed by a Bonferroni post-test was used in the ERG response analysis to compare the effects of stimulus intensity. A 1-way ANOVA followed by Tukey's test was used for the ERG response at the intensity of 2.1 log cd.s/

Investigative Ophthalmology & Visual Science

Downloaded From: https://iovs.arvojournals.org/pdfaccess.ashx?url=/data/journals/iovs/937362/ on 07/20/2018

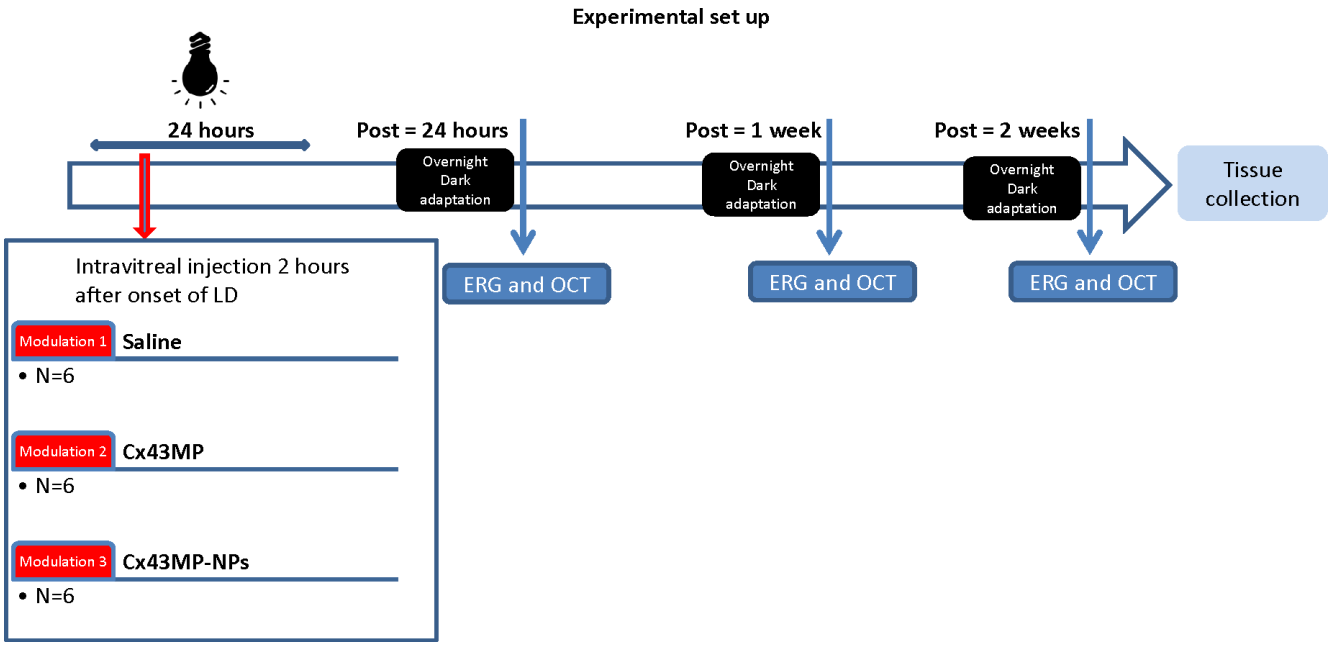

Figure 1. Diagram of the light exposure paradigm, intervention, and analysis time points.

m^2 in control versus light-damaged animals and also in the OCT data analysis.

Results

Localization of FITC-Cx43MP NPs in Choroid and Retina

To determine whether NPs delivered the peptide directly to retina and choroid, FITC-conjugated Cx43MP-NPs were injected into the vitreous. The whole-mount fluorescence signal and cross sections (Figs. 2A1, 2A2) analyzed 30 minutes post injection showed FITC in $CD45^+$ round cells in the choroid (Figs. 2B1–4). The labelling also showed FITC in the ganglion cell layer (GCL), OPL, and photoreceptors in cross sections (Fig. 2A3) and in whole mounts it was observed between but not colocalized with GFAP (Figs. 2C1–4). The fluorescent label was seen around blood vessels, mainly in the choroid, but also in the RPE (Fig. 2B) and in the retinal nerve fiber layer (Fig. 2C). This demonstrates that the tagged extracellular acting peptide was able to penetrate at least the inner retinal layers and that IVT injection allows consistent delivery of the peptide to the RPE and choroid.[46]

Effect of Sustained Cx43MP Delivery on Electroretinograms

Representative mixed ERG waveforms of each animal group at 2 weeks post light damage are shown in Figure 3A. The ERG allows assessment of changes in the function of the outer retina (a-wave) and inner retina (b-wave) and deciphering of the rod and cone pathway function using a range of light intensities. Compared with saline-injected animals, retinal function in the light-damaged rats did not improve at any of the time points studied (up to 2 weeks). Twenty-four hours after injection of the drug in the light-damaged rats, there were no significant differences between the Cx43MP-, Cx43MP-NP–, and the saline-injected groups in the a-wave (Figs. 3B, 3C). Significant improvements in mixed a-wave amplitude (rod and cone photoreceptors) in both Cx43MP- and Cx43MP-NP–treated animals at intensities of 1.1 to 2.1 log cd.s/m^2 were first detected at 1 week post treatment ($P < 0.001$, Figs. 3B, 3C). At 2 weeks post treatment, both Cx43MP and Cx43MP-NP groups showed a significant increase in rod and cone response (mixed a-wave amplitude) (Figs. 3B, 3C). Rats treated with Cx43MP had almost a 200-μV (on average) improvement in ERG a-wave compared with saline-injected rats at intensities of 1.1 to 2.1 log cd.s/m^2 ($P < 0.001$; Fig. 3B), but the improvement was bigger (more than 400 μV) in Cx43MP-NP–treated eyes compared with saline at intensities of 0.1 to 2.1 log cd.s/m^2 ($P < 0.001$; Fig. 3C). Table 2 shows the results of statistical comparison made between ERG results in Cx43MP- and Cx43MP-NP–treated animals. It shows that the improvement in b-wave of the ERG at 1 week post treatment reflects activation of the ON-bipolar cell pathway (rod and cone driven).[47] While this rescue persisted at 2 weeks post treatment, a-wave improved only at 2 weeks, suggesting that functional recovery of photoreceptors (both cones and rods) was considerable only 2 weeks post treatment.

No significant difference in mixed b-wave amplitude (cone and rod pathways) was detected at 24 hours post treatment (Figs. 3D, 3E). Further analysis on mixed b-wave amplitude in the ERG showed a significant increase only for intensity 1.1 log cd.s/m^2 for the Cx43MP group compared with saline ($P < 0.01$; Fig. 3D), suggesting that most changes were in the rod and cone function. A significant improvement in the Cx43MP-NP–treated group 1 week post treatment was seen for intensities 1.1 log cd.s/m^2 ($P < 0.05$) and from 1.6 to 2.1 log cd.sm^2 ($P < 0.01$; Fig. 3E). An overt improvement on inner retinal function demonstrated by an increased mixed b-wave amplitude throughout all stimulus intensities was found at 2 weeks post treatment in both Cx43MP- and Cx43MP-NP–treated animals compared with saline-injected rats ($P < 0.001$; Figs. 3D, 3E). NP-treated eyes showed an additional increase of approximately 200 μV in the absolute amplitude of the b-wave compared to native Cx43MP-treated eyes (compare Figs. 3D, 3E).

The ERG PIII component can be reconstructed from bright-flash ERG responses using the phototransduction model, and PII can be estimated by subtracting the estimated PIII.[48] Isolated rod PIII (rod photoreceptor function only) and rod PII

Investigative Ophthalmology & Visual Science

Downloaded From: https://iovs.arvojournals.org/pdfaccess.ashx?url=/data/journals/iovs/937362/ on 07/20/2018

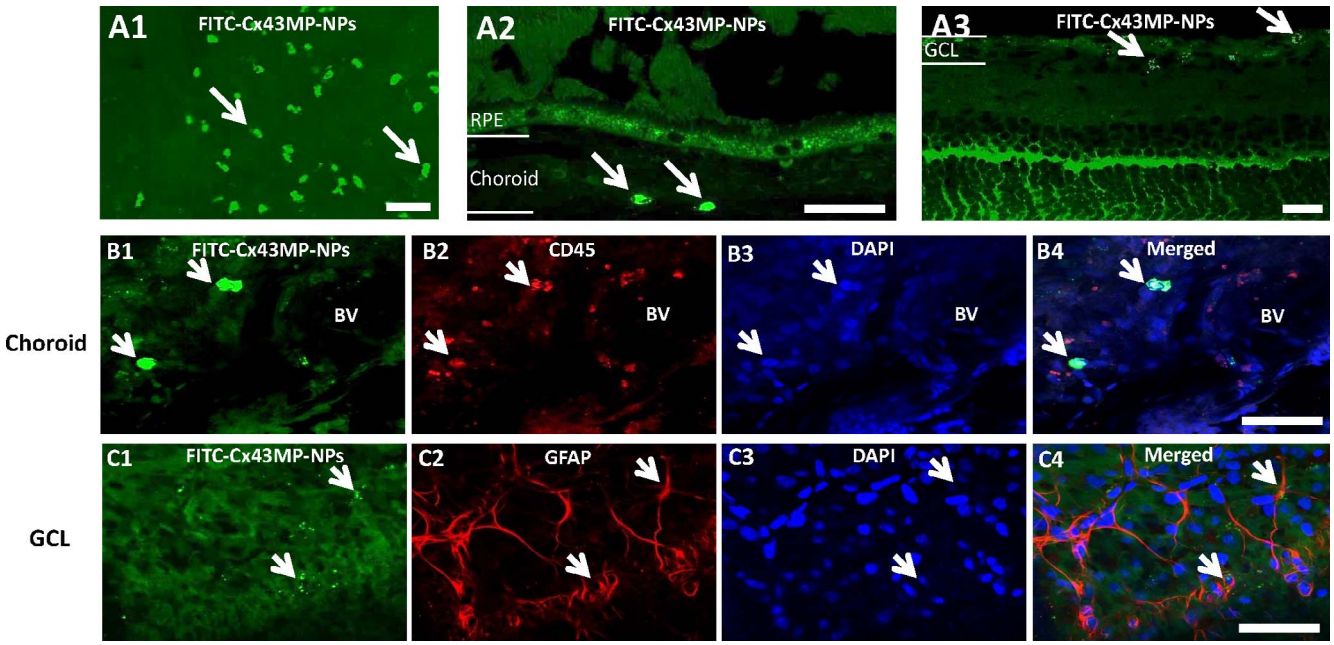

Figure 2. The location of FITC-Cx43MP-NPs injected in the vitreous in light-damaged rats. Eyes were enucleated 30 minutes post injection. In a whole mount, FITC was seen in the choroid (**A1**), and cross sections of the eye show FITC label in the choroid (**A2**) and in the GCL, OPL, and photoreceptors (**A3**). (**B1**) Whole-mount FITC label colocalizing with CD45 (**B2**), and DAPI (**B3**) shows FITC colocation with $CD45^{+}$ cells. Whole-mount FITC label (**C1**) did not extensively colocalize with GFAP (**C2**) or DAPI (**C3**) in the GCL layer. *Scale bar*: 50 µm.

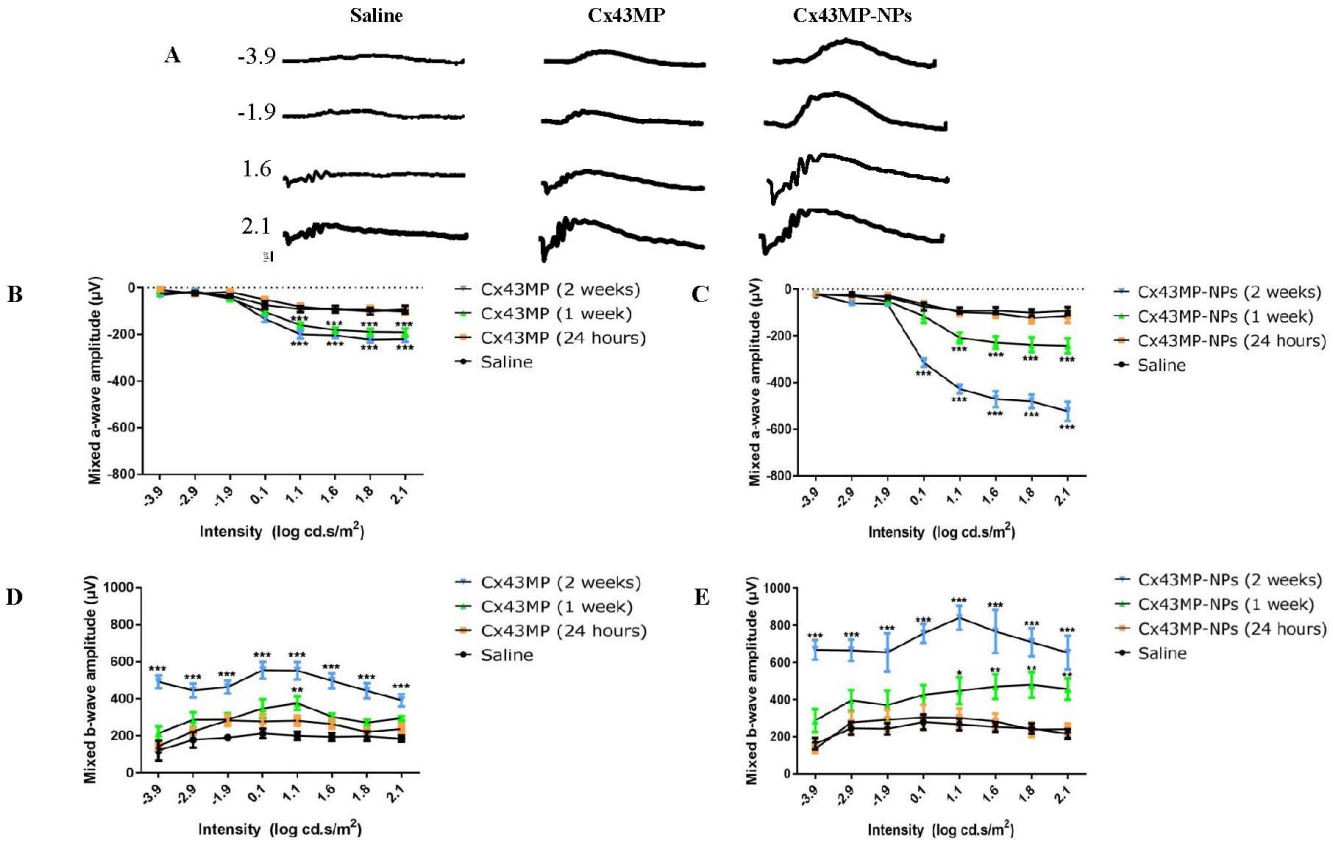

Figure 3. Representative ERG waveforms for light intensities ranging from −3.9 to 2.1 log cd.s/m^2 in saline-injected, Cx43MP-, or Cx43MP-NP–treated light-damaged rats (**A**). The effects of Cx43MP (**B**) and Cx43MP-NPs (**C**) on mixed a-wave amplitude; mixed b-wave amplitude effect of Cx43MP (**D**) and Cx43MP-NPs (**E**). Data for saline-injected light-damaged rats at 24 hours and 1 week are similar (nonsignificantly different) to those at 2 weeks. Statistical analysis was conducted using ANOVA, followed by Tukey's multiple post hoc test. Significant values in comparison with saline treatment are indicated with *asterisks*: $^{*}P < 0.05$; $^{**}P < 0.01$; $^{***}P < 0.001$.

Investigative Ophthalmology & Visual Science

Downloaded From: https://iovs.arvojournals.org/pdfaccess.ashx?url=/data/journals/iovs/937362/ on 07/20/2018

Table 2. Statistical Comparison Between Single-Injection Cx43MP and Cx43MP-NP ERG Results

	Statistical Analysis 1-Way ANOVA		
Time Post Intervention	**Cx43MP vs. Saline**	**Cx43MP-NPs vs. Saline**	**Cx43MP vs. Cx43MP-NPs**
Mixed a-wave amplitude			
24 h	NS	NS	NS
1 wk	$P = 0.0170$ 1.1 to 2.1 log cd.s/m^2	$P = 0.0014$ 0.1 to 2.1 log cd.s/m^2	NS
2 wk	$P < 0.001$ 0.1 to 2.1 log cd.s/m^2	$P < 0.001$ 0.1 to 2.1 log cd.s/m^2	$P < 0.001$ 0.1 to 2.1 log cd.s/m^2
Mixed b-wave amplitude			
24 h	NS	NS	NS
1 wk	$P = 0.0341$ 1.1 log cd.s/m^2	$P = 0.0213$ 1.0 to 1.1 log cd.s/m^2 $P = 0.0094$ 1.6 to 2.1 log cd.s/m^2	$P = 0.0156$ −2.9 to 1.1 log cd.s/m^2 $P = 0.0076$ 1.6 to 2.1 log cd.s/m^2
2 wk	$P < 0.001$ −3.9 to 2.1 log cd.s/m^2	$P < 0.001$ −3.9 to 2.1 log cd.s/m^2	$P < 0.001$ −3.9 to 2.1 log cd.s/m^2
Rod PIII amplitude			
24 h	NS	NS	NS
1 wk	NS	$P = 0.0102$	NS
2 wk	$P < 0.001$	$P < 0.001$	$P = 0.023$
Rod PII amplitude			
24 h	NS	NS	NS
1 wk	NS	$P = 0.0334$	NS
2 wk	NS	$P = 0.0092$	NS
Cone PII amplitude			
24 h	NS	NS	NS
1 wk	NS	$P = 0.0012$	NS
2 wk	$P = 0.0098$	$P = 0.042$	NS

NS, nonsignificant.

(rod pathway only) as well as cone PII (cone pathway) waveforms at the highest stimulus intensity (2.1 log cd.s/m^2) were analyzed and exhibited progressive recovery of the rod and cone post-photoreceptor activity for the Cx43MP-NP group compared to the saline-injected group (Figs. 4A, 4C). In the Cx43MP-NP–treated animals, cone PII recovery was demonstrated as early as 1 week post treatment (Fig. 4C) and improvements were seen on all rod PIII and PII and cone PII functions by 2 weeks post treatment (Figs. 4A, 4C). A progressive improvement as a function of time was not detected for Cx43MP-treated animals, and only 2 weeks post treatment results are shown (Figs. 4A–C). Cx43MP-treated eyes showed significant improvement on rod PIII and cone PII functions at 2 weeks post treatment compared with saline-injected eyes ($P < 0.001$; Fig. 4A) and ($P < 0.01$; Fig. 4C) but not in rod PII amplitude.

Effect of Sustained Cx43 Delivery on Retinal and Choroid Structure

Analysis of retinal and choroidal thickness was obtained from in vivo OCT scans at 2 weeks post treatment (Fig. 5). Both Cx43MP- and Cx43MP-NP–treated eyes showed a significant improvement in choroid and retinal thickness 2 weeks post light damage (Figs. 5A, 5B). OCT imaging showed that the choroid was significantly thinner in the light-damaged saline-injected eyes 2 weeks post treatment compared to imaging prior to damage ($P < 0.01$; Fig. 5C). The retina was also thinner in the saline-injected group compared to before damage (Fig. 5A), with the loss of retinal thickness mainly due to significant thinning of the outer nuclear layer (ONL; $P < 0.001$; Fig. 5D). Both Cx43MP-NP and Cx43MP preserved retinal structure (Figs. 5B, 5D). Cx43MP-NP–treated eyes retained full choroid thickness (Fig. 5C); eyes treated with a single dose of native Cx43MP, however, did not show preservation of choroidal thickness, with the thickness being similar to that in the saline group and significantly thinner than preinjury ($P < 0.01$; Fig. 5C).

We also monitored the effect of saline injection or drug treatment on retinal and choroidal thickness changes over time (Fig. 6). In saline-injected animals, intense light exposure caused an immediate change in the ONL thickness, previously reported to be due to death of photoreceptor cells,[49,50] that deteriorated further over the course of 2 weeks. Neither Cx43MP- nor Cx43MP-NP-treated animals showed a change in ONL thickness over the first week, although the Cx43MP rats did have a slight decrease in ONL thickness at the end of 2 weeks post injury (Fig. 6A). This decrease was nonsignificant compared to preinjury retinas. Light-exposed drug-treated retinal structure was significantly preserved compared to saline-injected light-exposed eyes (Fig. 6A). Conversely, light exposure caused a significant increase in choroidal thickness in saline-injected animals 24 hours after injury, followed by a reduction in thickness over the next 2 weeks (Fig. 6B). In comparison, Cx43MP-NP–treated rats had no significant fluctuation in choroidal thickness at any time point over the 2 weeks (Fig. 6B). However, Cx43MP–treated eyes had a decrease in choroidal thickness from 24 hours to 2 weeks compared with the Cx43MP-NP–treated rats (or choroidal thickness prior to injury; Fig. 6B).

Treatment Effect on Connexin43 Expression, Retinal Gliosis, and Inflammation

The effect of Cx43MP and Cx43MP-NPs on inflammation in the retina and choroid was investigated using immunohistochemical markers for GFAP (marker for astrocytes and Müller cell activation), CD45 (common lymphocyte antigen), and Cx43

Investigative Ophthalmology & Visual Science

Downloaded From: https://iovs.arvojournals.org/pdfaccess.ashx?url=/data/journals/iovs/937362/ on 07/20/2018

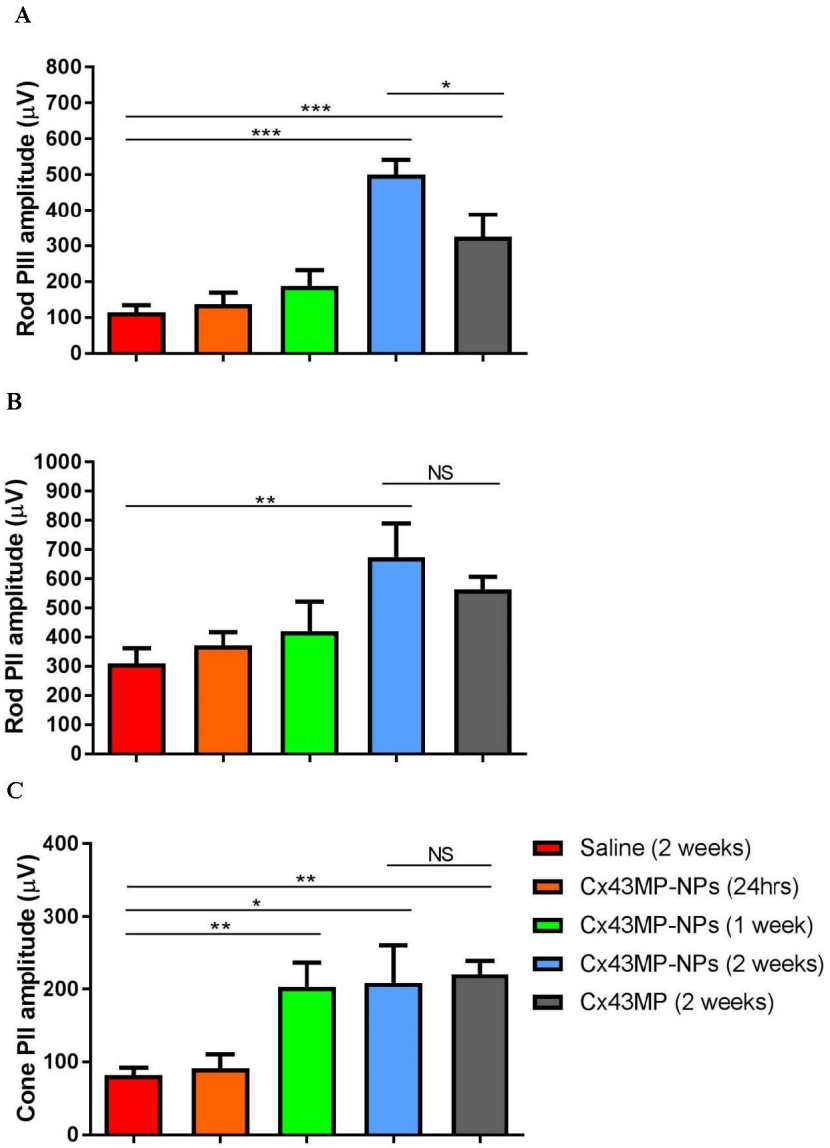

FIGURE 4. The effect of saline, Cx43MP-NPs, or Cx43MP on rod PIII amplitude (**A**), rod PII amplitude (**B**), and cone PII amplitude (**C**) of the electroretinogram. Statistical analysis was conducted using ANOVA, followed by Tukey's multiple post hoc test. Significant values in comparison with saline treatment are indicated with *asterisks*: $^{*}P < 0.05$; $^{**}P < 0.01$; $^{***}P < 0.001$.

(hemichannel protein) in tissues collected 2 weeks post light damage and saline or drug treatment (Fig. 7).

Cx43MP-NP–treated rats had less Cx43 immunoreactivity in the choroid compared with saline-injected or Cx43MP-treated eyes (Figs. 7A–C). There were also fewer CD45-positive cells in the choroid in Cx43MP-NP–treated animals compared with saline-injected animals (Figs. 7D, 7F). Treatment with Cx43MP also resulted in fewer CD45-positive cells in the choroid (Fig. 7E), although there were more than in the Cx43MP-NP–treated eyes (Fig. 7F). GFAP was used to determine the effect of Cx43MP and Cx43MP-NPs on astrocyte and Müller cell activation (Figs. 7G–I). Cx43MP-NP–treated rats had normal (preinjury) levels of GFAP label in the GCL (Fig. 7I). However, saline-injected animals showed a marked increase in GFAP expression in both the GCL and within Müller cells, indicating that these had become activated (Fig. 7G). The extent of GFAP immunoreactivity was less in Cx43MP-treated eyes (Fig. 7H) compared to saline-injected retina (Fig. 7G) but was more extensive than in Cx43MP-NP–treated rats (Fig. 7I). Taken together, these results suggest that there is a strong association between functional recovery and morphologic improvement with Cx43MP-NP treatment, especially over saline-injected controls, but also over eyes treated with Cx43MP alone.

DISCUSSION

This study was conducted to determine the effect of sustained Cx43MP release from NPs on the light-damaged rat retina in comparison with a single dose of native Cx43MP or with saline-injected control eyes. Nanoparticles allowed quick tissue distribution and slow release of mimetic peptide[21] resulting in improved retinal function, preserved retinal morphology, and reduced inflammation when followed through to 2 weeks after a single treatment. A single injection of Cx43MP alone was also beneficial, but improvements were more modest.

Prior studies have shown that administration of Cx43MP decreased inflammation and oxidative stress in this light-damaged rat retina model, but two injections of the peptide were required (2 hours post onset and at the end of the 24-

Investigative Ophthalmology & Visual Science

Downloaded From: https://iovs.arvojournals.org/pdfaccess.ashx?url=/data/journals/iovs/937362/ on 07/20/2018

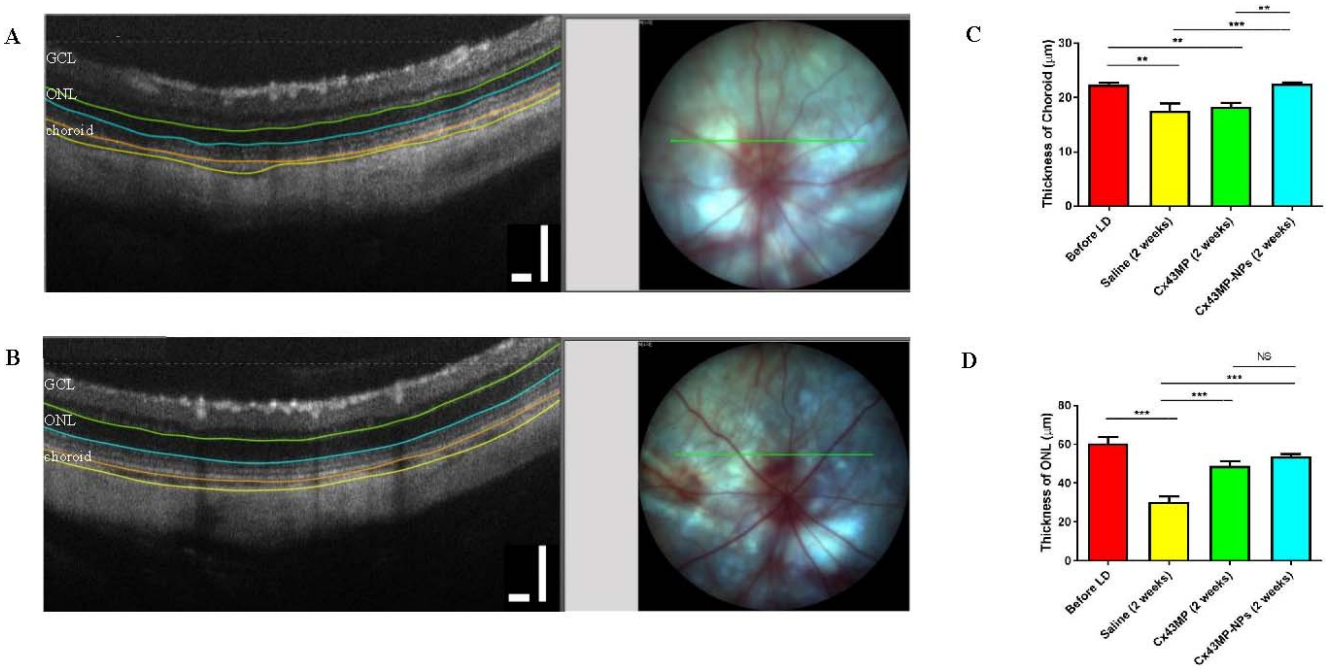

Figure 5. Effect of saline and Cx43MP-NP treatment on light-damaged rat retinal and choroidal thickness. Representative fundus and optical coherence tomography (OCT) images of the saline group (**A**) and the Cx43MP-NP–treated group (**B**). The *green line* on the fundus image represents the exact scanning location of the cross-sectional OCT image. The thickness of the choroid (**C**) and the ONL (**D**) were measured ($n = 6$ per group). Data are expressed as mean ± standard error of the mean. *Scale bar*: 100 μm. Significant values are indicated with *asterisks*: $^{**}P < 0.01$; $^{***}P < 0.001$.

hour light exposure period) in order to decrease the light-induced chorioretinal damage.[5] In the present study, a single injection of Cx43MP-NPs improved retinal function over the long term. Drug bioavailability was attained using NPs as the delivery system. These are capable of transretinal passage after IVT injection[51] and enable drug delivery into the RPE and choroid as shown in this study by the imaging of fluorescence-tagged peptides present in these layers within 30 minutes of administration. In this study, we cannot differentiate between transretinal passage and other passage mechanisms. It is possible that NPs were delivered to the choroid following endocytosis into Müller cells at the inner limiting membrane, followed by exocytosis at the external limiting membrane and into the interphotoreceptor matrix as has been previously proposed.[52] In any case, administration of the Cx43MP-NPs 2 hours after initiation of intense light exposure was effective at reducing the initial wave of damage that is characteristic of this animal model.[11] Progressive degradation of NPs then allowed slow release of Cx43MP to prevent photoreceptor loss and extensive retinal remodeling that are otherwise features of this disease model.[53–55]

PLGA are biodegradable polymers extensively used in ocular studies and also in pharmaceutical drug delivery studies as drug carriers.[56,57] Previous studies have shown that particles loaded with Cx43MP release the drug in a triphasic manner—an initial burst (49.5%), a long sustained period of slow release, and a final short burst when particles break down with Cx43MP release for up to 63 days.[21] In a more acute (shorter insult) retina ischemia–reperfusion model these NPs also proved effective,[21] most likely owing to the prolonged peptide release over time. Despite a slight delay in functional recovery compared with delivery of the drug in solution, the Cx43MP-NPs resulted in retinal structure and function protection. The long-term effect of slowly released Cx43 had an outcome similar to the effect of double injections of native Cx43MP in our previous study, suggesting a need to act on sequential critical damaging events that occur in this model.[58] PLGA has Food and Drug Administration (FDA) approval for the delivery of some ocular drugs, which, based on our studies, combined with Cx43, should be applicable in humans.[59]

In the long term, Cx43MP-NP treatment restored ERG function and immunolabeling with stress markers showing no alteration in glial reactivity. These results are consistent with data obtained in a previous, double-injection Cx43MP study.[5,11] Both a-wave, reflecting photoreceptor function, and b-wave, representing mainly bipolar cell function in the inner retina,[60] were spared. In this study, Cx43MP-NPs also improved the amplitude of rod and cone PIII and PII waveforms, which can be explained as neuroprotection of rod cells in the outer retina and rod bipolar cells and amacrine cells in the inner retina, respectively. A similar improvement in the rod pathway was associated with treatment of the light-damaged eye with mimetic peptide in saline.[11] Although the effect of Cx43MP on rod and cone pathways is still not clear, most of our experiments suggest that there is inflammation and Cx43 expression-mediated damage to the photoreceptors.[11]

The choroid plays a key role in preventing retinal damage. We have found an increase in choroidal thickness soon after light damage that is associated with an increased infiltration of leukocytes.[11] However, after 1 week, choroidal thickness decreased. This finding is consistent with findings of past studies indicating that the thinning of the choroid is associated with $CD8^+$ cytotoxic T lymphocytes infiltrating toward the retina and choroid interface in mice and albino rats.[61,62] This infiltration of T lymphocytes could exert deleterious effects on the choroid, RPE, and retina environments.[61,63] In this study, reduced Cx43 levels were seen as in previous studies, indicating that there is a reduced inflammatory response (the peptide does not in itself reduce Cx43 expression).[11] Furthermore, the hallmarks of retinal stress and upregulation of GFAP in astrocytes and Müller cells (signs of reactive gliosis)[64] were diminished with Cx43MP-NP treatment. It appears that the mimetic peptide reduces the inflammatory process that leads to retinal damage in this model.[11,49] The

Investigative Ophthalmology & Visual Science

Downloaded From: https://iovs.arvojournals.org/pdfaccess.ashx?url=/data/journals/iovs/937362/ on 07/20/2018

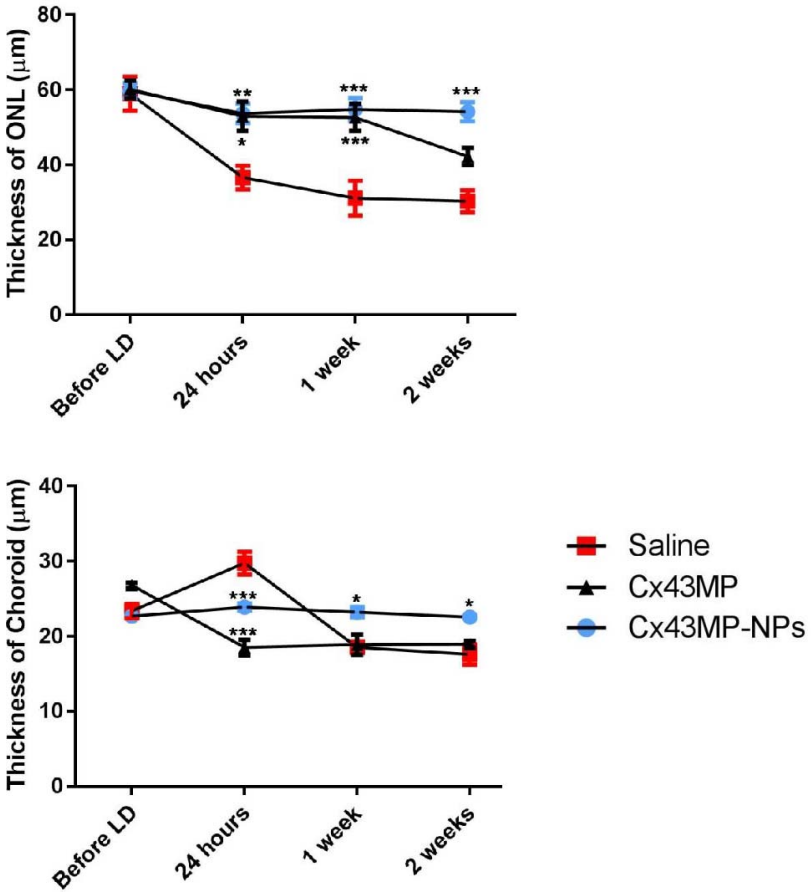

Figure 6. Quantification of retinal and choroidal thickness before light damage and up to 2 weeks post light damage in saline-, Cx43MP-, or Cx43MP-NP–treated eyes. The graphs show the changes in thickness of the ONL (**A**) and choroid (**B**) with $n = 6$ per group. Data are expressed as mean ± standard error of the mean. Significant values are indicated with *asterisks*: $^{*}P < 0.05$; $^{**}P < 0.01$; $^{***}P < 0.001$.

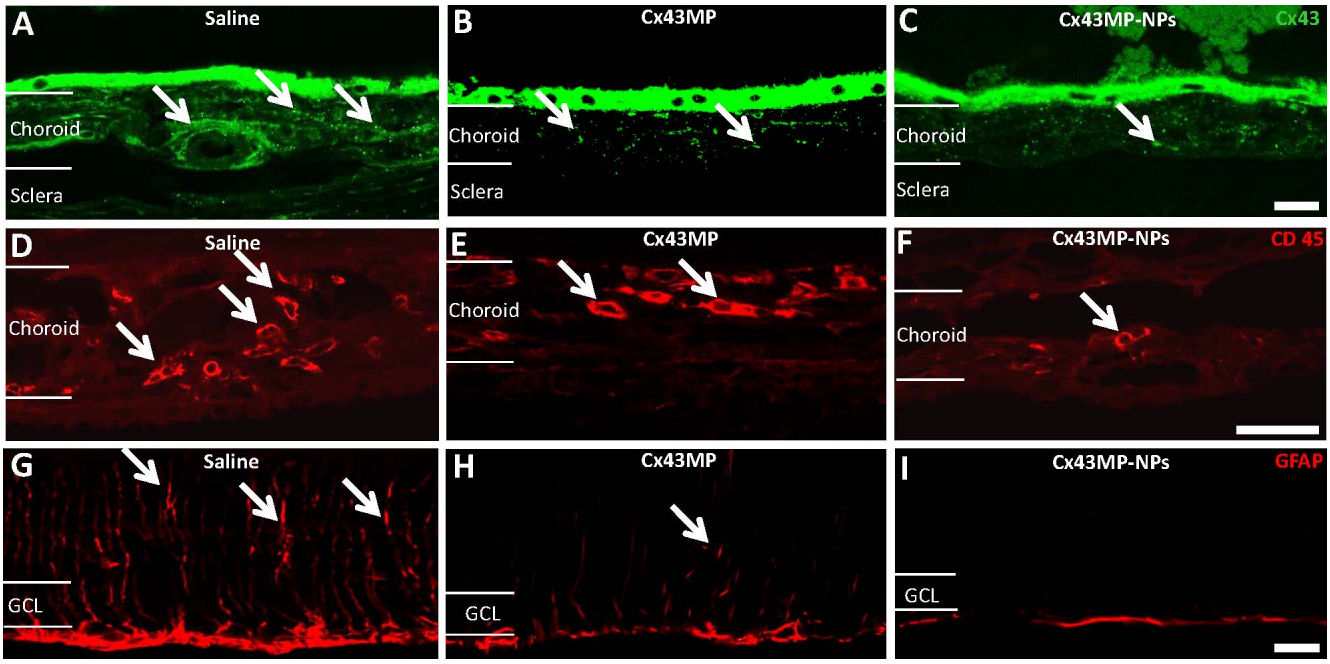

Figure 7. Cx43MP-NP–treated rat eyes showed less Cx43 immunoreactivity in the choroid (**C**) compared to native Cx43MP- (**B**) and saline-injected rats (**A**). CD45-immunolabelled cells were fewer in number in the choroid of Cx43MP-NP–treated rats (**F**) compared to native Cx43MP- (**E**) and saline-injected rats (**D**). GFAP immunoreactivity did not increase in the retina of Cx43MP-NP–treated rats (**I**) compared with native Cx43MP- (**H**) or saline-injected rats (**G**). *Scale bar*: 50 μm.

Investigative Ophthalmology & Visual Science

Downloaded From: https://iovs.arvojournals.org/pdfaccess.ashx?url=/data/journals/iovs/937362/ on 07/20/2018

choroid and retina have resident immune cells and are known to quickly react to invading agents.[65] In fact, accumulating evidence suggests that numerous aberrant macrophages invade the choroid and the retina in light-damaged eyes.[66] We observed increased $CD45^+$ cells in the choroid, some of them likely to be macrophages. Thus, it is possible that the therapy is regulating specific macrophage cell activity, preventing downstream inflammatory damage. The reduction in $CD45^+$ leukocytes in the choroid as a result of treatment may be important; interleukin release from these cells may be the cause of increased GFAP expression in Müller cells in an attempt to protect the retina.[67] Sustained release of Cx43MP from NPs works better than the free peptide, suggesting that different/later stages of the inflammatory response may be the target of the therapeutic treatment.

Previous studies have shown that Cx43MP blocks the uncontrolled opening of hemichannels without uncoupling gap junctions,[68,69] and that these Cx43 hemichannels are membrane pores with a significant role in the development of inflammation. The intense light exposure rat model has alterations in endothelial cells of the choriocapillaris, leading to inflammation via Cx43 hemichannel opening, controlled by mimetic peptides that block uncontrolled opening. In fact, peptide5 reduced vessel leak and inflammation while it improved function in brain injury models.[16,70] Our study also suggests that one site of action may be RPE cells, which through the release of growth factors may cause sustained pathology in the choroid, secreting proinflammatory molecules associated with the inflammasome pathway.[16] Under resting conditions, Cx43 hemichannels have a low open probability but in the presence of molecules recognizable by the innate immune system, the increased assembly and opening of hemichannels can be triggered to induce release of proinflammatory molecules and ATP.[13,16]

It is likely that at least some of the cells that express Cx43 hemichannels and contribute to RPE activation of the inflammasome are resident macrophages,[12,13,71,72] further supporting that the intervention with Cx43MP is regulating inflammation. Intervention in the ischemia–reperfusion rat model using a Cx43 channel blocking mimetic peptide reduced the number of inflammatory cells in the tissue and restored retinal function.[23] The concentration of Cx43 peptide used in the animal model meant we were specifically targeting Cx43 pathological pores rather than gap junctions between cells in adjacent tissues. The therapy is effectively acting on a specific step in the inflammatory process to prevent retinal damage from an extensive immune response. The comparison between the two formulations we used supports our view that sustained mimetic peptide delivery (with NPs) is active at a stage of the pathology when native peptide may be already degraded. In the light damage rat model state of chronic inflammation, typical of early AMD, sustained release of mimetic peptide is able to break a pathological hemichannel-mediated inflammatory cycle that is a significant mechanism of the pathology.

In conclusion, these results suggest that a single injection of Cx43MP loaded into NPs to provide sustained peptide delivery preserves function and morphology of the light-damaged eye, acting to reduce the inflammatory response that is elicited in the retina and the choroid soon after light damage, and is connexin hemichannel mediated. The evidence suggests that overt inflammation and Cx43 expression are intimately related to retinal light damage, and Cx43MP may be an effective therapy when incorporated into NPs for the long-term treatment of retinal degeneration and to reduce possible ocular complications associated with repeated IVT injections.

Acknowledgments

Supported by a grant from Lottery Health Research (9113 3707605); CRG acknowledges support from Wendy and Bruce Hadden. IDR is supported by the Buchanan Charitable Foundation. NMN holds a PhD scholarship from Ministry of Higher Education Malaysia.

Disclosure: **N. Mat Nor**, None; **C.X. Guo**, None; **I.D. Rupenthal**, None; **Y.-S. Chen**, None; **C.R. Green**, None; **M.L. Acosta**, None

References

1. Wang Y, Wang VM, Chan CC. The role of anti-inflammatory agents in age-related macular degeneration (AMD) treatment. *Eye (Lond)*. 2011;25:127–139.
2. Hollyfield JG, Bonilha VL, Rayborn ME, et al. Oxidative damage-induced inflammation initiates age-related macular degeneration. *Nat Med*. 2008;14:194–198.
3. Kauppinen A, Paterno JJ, Blasiak J, Salminen A, Kaarniranta K. Inflammation and its role in age-related macular degeneration. *Cell Mol Life Sci*. 2016;73:1765–1786.
4. Penfold PL, Madigan MC, Gillies MC, Provis JM. Immunological and aetiological aspects of macular degeneration. *Prog Retin Eye Res*. 2001;20:385–414.
5. Guo CX, Mat Nor MN, Danesh-Meyer HV, et al. Connexin43 mimetic peptide improves retinal function and reduces inflammation in a light-damaged albino rat model. *Invest Ophthalmol Vis Sci*. 2016;57:3961–3973.
6. Bennett MV, Zheng X, Sogin ML. The connexins and their family tree. *Soc Gen Physiol Ser*. 1994;49:223–233.
7. Nagy JI, Rash JE. Connexins and gap junctions of astrocytes and oligodendrocytes in the CNS. *Brain Res Brain Res Rev*. 2000;32:29–44.
8. Ezan P, Andre P, Cisternino S, et al. Deletion of astroglial connexins weakens the blood-brain barrier. *J Cereb Blood Flow Metab*. 2012;32:1457–1467.
9. De Bock M, Culot M, Wang N, et al. Connexin channels provide a target to manipulate brain endothelial calcium dynamics and blood-brain barrier permeability. *J Cereb Blood Flow Metab*. 2011;31:1942–1957.
10. De Bock M, Vandenbroucke RE, Decrock E, Culot M, Cecchelli R, Leybaert L. A new angle on blood-CNS interfaces: a role for connexins? *FEBS Lett*. 2014;588:1259–1270.
11. Guo CX, Tran H, Green CR, Danesh-Meyer HV, Acosta ML. Gap junction proteins in the light-damaged albino rat. *Mol Vis*. 2014;20:670–682.
12. Beyer EC, Steinberg TH. Evidence that the gap junction protein connexin-43 is the ATP-induced pore of mouse macrophages. *J Biol Chem*. 1991;266:7971–7974.
13. Eugenin EA, Branes MC, Berman JW, Saez JC. TNF-alpha plus IFN-gamma induce connexin43 expression and formation of gap junctions between human monocytes/macrophages that enhance physiological responses. *J Immunol*. 2003;170:1320–1328.
14. Decrock E, De Vuyst E, Vinken M, et al. Connexin 43 hemichannels contribute to the propagation of apoptotic cell death in a rat C6 glioma cell model. *Cell Death Differ*. 2009;16:151–163.
15. Willebrords J, Crespo Yanguas S, Maes M, et al. Connexins and their channels in inflammation. *Crit Rev Biochem Mol Biol*. 2016;51:413–439.
16. Kim Y, Davidson JO, Gunn KC, Phillips AR, Green CR, Gunn AJ. Role of hemichannels in CNS inflammation and the inflammasome pathway. *Adv Protein Chem Struct Biol*. 2016;104:1–37.
17. Yi C, Mei X, Ezan P, et al. Astroglial connexin43 contributes to neuronal suffering in a mouse model of Alzheimer's disease. *Cell Death Differ*. 2016;23:1691–1701.

Downloaded From: https://iovs.arvojournals.org/pdfaccess.ashx?url=/data/journals/iovs/937362/ on 07/20/2018

18. O'Carroll SJ, Alkadhi M, Nicholson LF, Green CR. Connexin 43 mimetic peptides reduce swelling, astrogliosis, and neuronal cell death after spinal cord injury. *Cell Commun Adhes*. 2008; 15:27–42.
19. O'Carroll SJ, Gorrie CA, Velamoor S, Green CR, Nicholson LF. Connexin43 mimetic peptide is neuroprotective and improves function following spinal cord injury. *Neurosci Res*. 2013;75:256–267.
20. Mao Y, Tonkin RS, Nguyen T, et al. Systemic administration of connexin43 mimetic peptide improves functional recovery after traumatic spinal cord injury in adult rats. *J Neurotrauma*. 2017;34:707–719.
21. Chen YS, Green CR, Wang K, Danesh-Meyer HV, Rupenthal ID. Sustained intravitreal delivery of connexin43 mimetic peptide by poly(D,L-lactide-co-glycolide) acid micro- and nanoparticles – closing the gap in retinal ischaemia. *Eur J Pharm Biopharm*. 2015;95:378–386.
22. Davidson JO, Drury PP, Green CR, Nicholson LF, Bennet L, Gunn AJ. Connexin hemichannel blockade is neuroprotective after asphyxia in preterm fetal sheep. *PLoS One*. 2014;9: e96558.
23. Danesh-Meyer HV, Kerr NM, Zhang J, et al. Connexin43 mimetic peptide reduces vascular leak and retinal ganglion cell death following retinal ischaemia. *Brain*. 2012;135:506–520.
24. Davidson JO, Green CR, Nicholson LF, et al. Connexin hemichannel blockade improves outcomes in a model of fetal ischemia. *Ann Neurol*. 2012;71:121–132.
25. Retamal MA, Froger N, Palacios-Prado N, et al. Cx43 hemichannels and gap junction channels in astrocytes are regulated oppositely by proinflammatory cytokines released from activated microglia. *J Neurosci*. 2007;27:13781–13792.
26. Chen YS, Toth I, Danesh-Meyer HV, Green CR, Rupenthal ID. Cytotoxicity and vitreous stability of chemically modified connexin43 mimetic peptides for the treatment of optic neuropathy. *J Pharm Sci*. 2013;102:2322–2331.
27. O'Carroll SJ, Gorrie CA, Velamoor S, Green CR, Nicholson LFB. Connexin43 mimetic peptide is neuroprotective and improves function following spinal cord injury. *Neurosci Res*. 2013;75:256–267.
28. Prieto E, Perez S, Pablo LE, Garcia MA, Bregante MA. Vitreous pharmacokinetics and bioavailability of memantine after subtenon, intravenous, and intravitreal administration in rabbits. *J Ocular Pharm Ther*. 2014;30:392–399.
29. Gaudana R, Ananthula HK, Parenky A, Mitra AK. Ocular drug delivery. *AAPS J*. 2010;12:348–360.
30. Thassu D, Chader GJ. *Ocular Drug Delivery Systems: Barriers and Application of Nanoparticulate Systems*. Boca Raton: CRC Press; 2013:237–238.
31. Gaudana R, Jwala J, Boddu SH, Mitra AK. Recent perspectives in ocular drug delivery. *Pharm Res*. 2009;26:1197–1216.
32. Raghava S, Hammond M, Kompella UB. Periocular routes for retinal drug delivery. *Expert Opin Drug Deliv*. 2004;1:99–114.
33. Janoria KG, Gunda S, Boddu SH, Mitra AK. Novel approaches to retinal drug delivery. *Expert Opin Drug Deliv*. 2007;4:371–388.
34. Blanco E, Shen H, Ferrari M. Principles of nanoparticle design for overcoming biological barriers to drug delivery. *Nat Biotechnol*. 2015;33:941–951.
35. Robinson R, Viviano SR, Criscione JM, et al. Nanospheres delivering the EGFR TKI AG1478 promote optic nerve regeneration: the role of size for intraocular drug delivery. *ACS Nano*. 2011;5:4392–4400.
36. Herrero-Vanrell R, Bravo-Osuna I, Andres-Guerrero V, Vicario-de-la-Torre M, Molina-Martinez IT. The potential of using biodegradable microspheres in retinal diseases and other intraocular pathologies. *Prog Retin Eye Res*. 2014;42:27–43.
37. Chen YS, Alany RG, Young SA, Green CR, Rupenthal ID. In vitro release characteristics and cellular uptake of poly(D,L-lactic-co-glycolic acid) nanoparticles for topical delivery of antisense oligodeoxynucleotides. *Drug Deliv*. 2011;18:493–501.
38. Giordano GG, Chevez-Barrios P, Refojo MF, Garcia CA. Biodegradation and tissue reaction to intravitreous biodegradable poly(D,L-lactic-co-glycolic)acid microspheres. *Curr Eye Res*. 1995;14:761–768.
39. Moritera T, Ogura Y, Honda Y, Wada R, Hyon SH, Ikada Y. Microspheres of biodegradable polymers as a drug-delivery system in the vitreous. *Invest Ophthalmol Vis Sci*. 1991;32: 1785–1790.
40. Canadas C, Alvarado H, Calpena AC, et al. In vitro, ex vivo and in vivo characterization of PLGA nanoparticles loading pranoprofen for ocular administration. *Int J Pharm*. 2016; 511:719–727.
41. Gao Y, Sun Y, Ren F, Gao S. PLGA-PEG-PLGA hydrogel for ocular drug delivery of dexamethasone acetate. *Drug Dev Ind Pharm*. 2010;36:1131–1138.
42. Gupta H, Aqil M, Khar RK, Ali A, Bhatnagar A, Mittal G. Sparfloxacin-loaded PLGA nanoparticles for sustained ocular drug delivery. *Nanomedicine*. 2010;6:324–333.
43. Katara R, Sachdeva S, Majumdar DK. Enhancement of ocular efficacy of aceclofenac using biodegradable PLGA nanoparticles: formulation and characterization. *Drug Deliv Transl Res*. 2017;7:632–641.
44. Kalam MA, Alshamsan A. Poly (d, l-lactide-co-glycolide) nanoparticles for sustained release of tacrolimus in rabbit eyes. *Biomed Pharmacother*. 2017;94:402–411.
45. Vessey KA, Wilkinson-Berka JL, Fletcher EL. Characterization of retinal function and glial cell response in a mouse model of oxygen-induced retinopathy. *J Comp Neurol*. 2011;519:506–527.
46. Bourges J-L, Gautier SE, Delie F, et al. Ocular drug delivery targeting the retina and retinal pigment epithelium using polylactide nanoparticles. *Invest Ophthalmol Vis Sci*. 2003; 44:3562–3569.
47. Stockton RA, Slaughter MM. B-wave of the electroretinogram. A reflection of ON bipolar cell activity. *J Gen Physiol*. 1989; 93:101–122.
48. Hood DC, Birch DG. A computational model of the amplitude and implicit time of the b-wave of the human ERG. *Vis Neurosci*. 1992;8:107–126.
49. Rutar M, Provis JM, Valter K. Brief exposure to damaging light causes focal recruitment of macrophages, and long-term destabilization of photoreceptors in the albino rat retina. *Curr Eye Res*. 2010;35:631–643.
50. Noell WK, Walker VS, Kang BS, Berman S. Retinal damage by light in rats. *Invest Ophthalmol*. 1966;5:450–473.
51. Bejjani RA, BenEzra D, Cohen H, et al. Nanoparticles for gene delivery to retinal pigment epithelial cells. *Mol Vis*. 2005;11: 124–132.
52. Koo H, Moon H, Han H, et al. The movement of self-assembled amphiphilic polymeric nanoparticles in the vitreous and retina after intravitreal injection. *Biomaterials*. 2012; 33:3485–3493.
53. Marc RE, Jones BW, Watt CB, Vazquez-Chona F, Vaughan DK, Organisciak DT. Extreme retinal remodeling triggered by light damage: implications for age related macular degeneration. *Mol Vis*. 2008;14:782–806.
54. Organisciak DT, Vaughan DK. Retinal light damage: mechanisms and protection. *Prog Retin Eye Res*. 2010;29:113–134.
55. Stone J, Maslim J, Valter-Kocsi K, et al. Mechanisms of photoreceptor death and survival in mammalian retina. *Prog Retin Eye Res*. 1999;18:689–735.

Investigative Ophthalmology & Visual Science

Downloaded From: https://iovs.arvojournals.org/pdfaccess.ashx?url=/data/journals/iovs/937362/ on 07/20/2018

56. Chen YS, Green CR, Danesh-Meyer HV, Rupenthal ID. Neuroprotection in the treatment of glaucoma - a focus on connexin43 gap junction channel blockers. *Eur J Pharm Biopharm*. 2015;95:182–193.
57. Hua X, Tan S, Bandara HM, Fu Y, Liu S, Smyth HD. Externally controlled triggered-release of drug from PLGA micro and nanoparticles. *PLoS One*. 2014;9:e114271.
58. Masuda T, Shimazawa M, Hara H. Retinal diseases associated with oxidative stress and the effects of a free radical scavenger (Edaravone). *Oxid Med Cell Longev*. 2017;2017: 9208489.
59. Kompella UB, Amrite AC, Pacha Ravi R, Durazo SA. Nanomedicines for back of the eye drug delivery, gene delivery, and imaging. *Prog Retin Eye Res*. 2013;36:172–198.
60. Liu Y, McDowell CM, Zhang Z, Tebow HE, Wordinger RJ, Clark AF. Monitoring retinal morphologic and functional changes in mice following optic nerve crush. *Invest Ophthalmol Vis Sci*. 2014;55:3766–3774.
61. Camelo S, Calippe B, Lavalette S, et al. Thinning of the RPE and choroid associated with T lymphocyte recruitment in aged and light-challenged mice. *Mol Vis*. 2015;21:1051–1059.
62. Collier RJ, Wang Y, Smith SS, et al. Complement deposition and microglial activation in the outer retina in light-induced retinopathy: inhibition by a 5-HT1A agonist. *Invest Ophthalmol Vis Sci*. 2011;52:8108–8116.
63. Ferrington DA, Tran TN, Lew KL, Van Remmen H, Gregerson DS. Different death stimuli evoke apoptosis via multiple pathways in retinal pigment epithelial cells. *Exp Eye Res*. 2006;83:638–650.
64. Chang ML, Wu CH, Jiang-Shieh YF, Shieh JY, Wen CY. Reactive changes of retinal astrocytes and Müller glial cells in kainate-induced neuroexcitotoxicity. *J Anat*. 2007;210:54–65.
65. Yildirim Z, Ucgun NI, Yildirim F. The role of oxidative stress and antioxidants in the pathogenesis of age-related macular degeneration. *Clinics*. 2011;66:743–746.
66. Cringle SJ, Yu DY. Oxygen supply and consumption in the retina: implications for studies of retinopathy of prematurity. *Doc Ophthalmol*. 2010;120:99–109.
67. Rutar M, Natoli R, Chia RX, Valter K, Provis JM. Chemokine-mediated inflammation in the degenerating retina is coordinated by Müller cells, activated microglia, and retinal pigment epithelium. *J Neuroinflammation*. 2015;12:8.
68. O'Carroll SJ, Alkadhi M, Nicholson LF, Green CR. Connexin 43 mimetic peptides reduce swelling, astrogliosis, and neuronal cell death after spinal cord injury. *Cell Commun Adhes*. 2008; 15:27–42.
69. Kim Y, Griffin JM, Harris PW, et al. Characterizing the mode of action of extracellular Connexin43 channel blocking mimetic peptides in an in vitro ischemia injury model. *Biochim Biophys Acta*. 2017;1861:68–78.
70. Danesh-Meyer HV, Zhang J, Acosta ML, Rupenthal ID, Green CR. Connexin43 in retinal injury and disease. *Prog Retin Eye Res*. 2016;51:41–68.
71. Penfold PL, Killingsworth MC, Sarks SH. Senile macular degeneration: the involvement of immunocompetent cells. *Graefes Arch Clin Exp Ophthalmol*. 1985;223:69–76.
72. Glass AM, Snyder EG, Taffet SM. Connexins and pannexins in the immune system and lymphatic organs. *Cell Mol Life Sci*. 2015;72:2899–2910.
73. Kerr NM, Johnson CS, de Souza CF, et al. Immunolocalization of gap junction protein connexin43 (GJA1) in the human retina and optic nerve. *Invest Ophthalmol Vis Sci*. 2010;51: 4028–4034.

Investigative Ophthalmology & Visual Science

Downloaded From: https://iovs.arvojournals.org/pdfaccess.ashx?url=/data/journals/iovs/937362/ on 07/20/2018